Joule

Article

On-demand capacity extraction through thermo-electrochemical hysteresis in metastable Li-Cu alloy

Graphical abstract

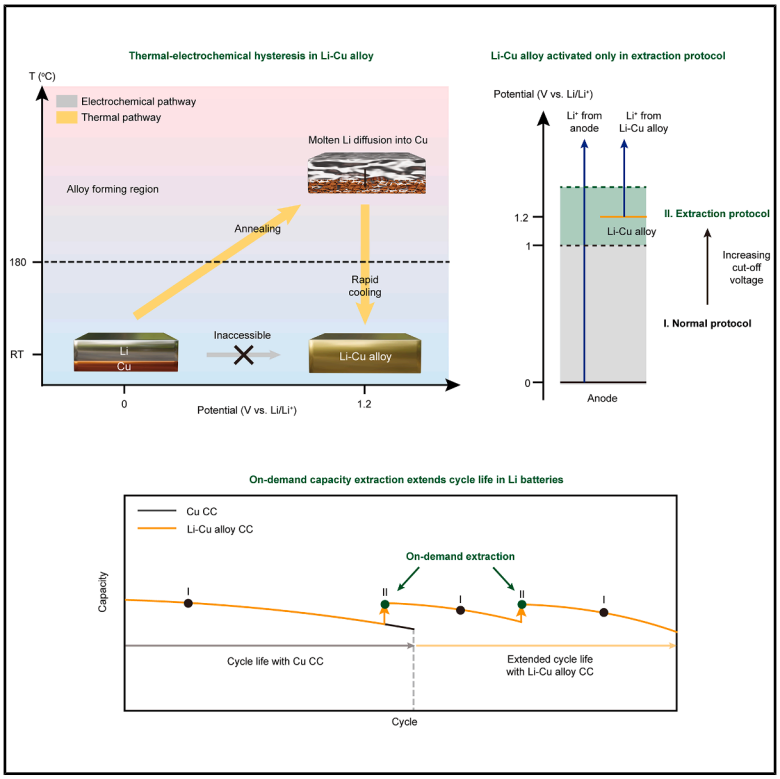

Highlights

- Metastable Li-Cu alloy stores lithium via thermo-electrochemical hysteresis
- The stored capacity stays inactive until released by a designed extraction protocol
- On-demand Li extraction during cycling extends cycle life in both LMBs and LIBs

Authors

Jun Ho Lee, Wenbo Zhang, Yusheng Ye, ..., Malhar Kute, Thomas P. Devereaux, Yi Cui

Correspondence

yicui@stanford.edu

In brief

Batteries steadily lose usable lithium as they cycle, as reactive lithium is consumed spontaneously—a key factor limiting how long they retain capacity. A metastable lithium-copper alloy, built into the current collector, stores lithium in reserve and keeps it dormant during operation. The stored lithium is released only when intentionally triggered, boosting the cell's capacity on demand and extending cycle life in both lithium-metal and lithium-ion batteries, illustrating how metastable materials can introduce functionalities to energy storage.

Lee et al., 2027, Joule *11*, 102632
February 17, 2027
https://doi.org/10.1016/j.joule.2026.102632

CellPress

Joule

CellPress

Article

On-demand capacity extraction through thermo-electrochemical hysteresis in metastable Li-Cu alloy

Jun Ho Lee,[1] Wenbo Zhang,[1] Yusheng Ye,[1] Sarah E. Holmes,[2] Eder G. Lomeli,[1,3] Sanzeeda Baig Shuchi,[4] Sang Cheol Kim,[1] Mun Sek Kim,[4] Junyoung Lee,[1] Il Rok Choi,[1] Donglin Li,[1] Huayue Ai,[2] Philaphon Sayavong,[2] Solomon T. Oyakhire,[4] Malhar Kute,[1,3] Thomas P. Devereaux,[1,3] and Yi Cui[1,3,5,6,*]

[1]Department of Materials Science and Engineering, Stanford University, Stanford, CA, USA
[2]Department of Chemistry, Stanford University, Stanford, CA, USA
[3]Stanford Institute for Materials and Energy Sciences, SLAC National Accelerator Laboratory, Menlo Park, CA, USA
[4]Department of Chemical Engineering, Stanford University, Stanford, CA, USA
[5]Department of Energy Science and Engineering, Stanford University, Stanford, CA, USA
[6]Lead contact
*Correspondence: yicui@stanford.edu
https://doi.org/10.1016/j.joule.2026.102632

CONTEXT & SCALE Lithium-ion and lithium-metal batteries consistently lose a fraction of their usable lithium during cycling, as reactive lithium reacts with electrolyte molecules to form the solid-electrolyte interphase, which contributes to the formation of electrically isolated "dead" lithium. This irreversible loss of active lithium is one of the fundamental challenges limiting capacity retention of batteries. Prelithiation—adding extra lithium to the cell components—can offset the initial loss, but the added lithium is typically released within the first few cycles and cannot be stored or supplied later, when the battery is degraded. A true lithium reservoir would instead store lithium safely, remain dormant during normal operation, and release lithium only when needed.

Here, we show that a metastable lithium-copper alloy can serve as such a reservoir. Prepared by a simple thermal treatment, the alloy is introduced directly as the current collector—an inactive part of the cell—and stores lithium in a state that is not accessible through electrochemistry at room temperature. Because the stored lithium is held at an unusually high potential, it stays electrochemically silent during ordinary cycling and is released only when a deliberately designed protocol activates it. This decoupling of storage from release, enabled by thermo-electrochemical hysteresis, allows lithium to be supplemented on demand at any stage of a battery's life, extending cycle life in both lithium-metal and lithium-ion configurations. This work demonstrates that, with appropriate optimization, metastable phases can be exploited to introduce added functionality to energy-storage materials at larger, practical scales.

SUMMARY

Metastable states provide unique opportunities to access functional materials inaccessible through conventional equilibrium pathways. Here, we employ this path dependency to enable safe storage and supplementation of capacity in lithium (Li) batteries, compensating for irreversible loss of Li caused by its high reactivity. We introduce a strategy of storing Li as a metastable Li-Cu alloy phase with characteristic thermo-electrochemical hysteresis—the phase is accessible only through a thermal process, inhibiting electrochemical re-alloying with Cu during cycling. The Li-Cu current collector (CC) demonstrates on-demand capacity extraction of up to 2 mAh cm^{-2} for extended cycle life in Li batteries. The high extraction potential of the Li-Cu alloy (1.2 V vs. Li/Li^+) allows intentional activation by a designed protocol while otherwise remaining inactive within the conventional operating window. This approach transforms CCs into a Li reservoir with on-demand capability via hysteretic pathways, offering a promising design platform for high-energy-density batteries.

Please cite this article in press as: Lee et al., On-demand capacity extraction through thermo-electrochemical hysteresis in metastable Li-Cu alloy, Joule (2026), https://doi.org/10.1016/j.joule.2026.102632

INTRODUCTION

Metastable states provide a unique opportunity to access material states with desirable properties that are challenging to reach through standard equilibrium chemistry. These states are typically achieved by following path-dependent transformations, and the final composition and crystal structure of materials are determined by the sequence of synthetic routes—thermal, chemical, or electrochemical. By exploring these non-equilibrium pathways—often referred to as synthetic hysteresis—materials can be stabilized in specific compositions without spontaneous relaxation. While this approach has already led to functional breakthroughs in fields like metallurgy,[1] magnetism,[2,3] and catalysis,[4] its application toward creating additional functionalities in energy storage by decoupling synthetic and activation pathways remains largely unexplored. In this context, such path-dependent pathways offer an effective strategy to effectively manage the active lithium (Li) inventory, which is the key to overcoming the fundamental limits of long-term capacity retention.

Retaining reversible capacity over longer cycles is a fundamental requirement for the development of Li batteries with high-energy density.[5] However, the continuous buildup of the solid-electrolyte interphase (SEI), a passivation layer formed by the decomposition of electrolyte at the strongly reducing anode surface, and accumulation of electrically isolated ("dead") Li are still remaining challenges that lead to persistent loss in the active Li inventory.[6–9] To mitigate the Li loss, approaches including electrolyte engineering,[10–13] artificial SEI,[14–16] and Li host materials[17,18] have been extensively designed to facilitate the formation of stable SEI layers. Despite these efforts, complete prevention of irreversible capacity loss is still not feasible within the current battery architecture.

Prelithiation, the introduction of extra Li capacity to battery cells, has emerged as a promising strategy for improving battery capacity.[19] The additional Li capacity in various forms, including prelithiation reagents to anodes and cathodes,[20–23] adding a thin Li metal on the anode,[18,24,25] or synthesizing Li-rich cathode materials,[26] compensates for the loss, thus improving initial Coulombic efficiency (ICE) and extending the life of the battery. Despite the recent progress, extraction potentials of these materials lie within the electrochemical operating window of electrodes, leading to an unavoidable Li release within the first few cycles, which precludes temporal control and long-term storage. A true reservoir should (1) store Li for longer cycles, (2) remain electrochemically inactive during cycling, and (3) release Li on demand when the battery is degraded. Enabling on-demand rejuvenation of reversible capacity at later cycles is desirable but not yet achieved.

Here, we propose Li-Cu alloy as a Li reservoir that can supplement capacity on demand in Li batteries. Thin Li-Cu alloy current collector (CC) prepared by thermal annealing provides controllable areal capacity ranging from 0.5 to 2 mAh cm^{-2}, and its properties, such as crystal structure and diffusion mechanism, are revealed by empirical and theoretical analyses. The high reduction potential of the Li-Cu alloy (1.2 V vs. Li/Li^+) enables both an increase in the chemical stability of the alloy compared with metallic Li (Li^0) and selective access to the Li source by elevating the anode potential. This prelithiated capacity can be extracted without re-alloying at any stage during cycling to reach ~100% and 210% of ICE for graphite (Gr) anodes and Li metal anodes, respectively, implying applicability in both Li-ion batteries (LIBs) and Li metal batteries (LMBs). Lastly, we demonstrate the on-demand Li extraction of Li-Cu CC in full cells using $LiNi_{0.8}Mn_{0.1}Co_{0.1}O_2$ (NMC811) cathodes with a considerate design of discharging protocols and rejuvenate cell capacity during cycling. Our concept of utilizing a metastable Li-Cu alloy phase as a CC not only improves the chemical stability of Li and provides a boost in capacity when needed for prolonged cycle life but also concurrently utilizes the inactive component of the battery.

RESULTS AND DISCUSSION

Design of metastable Li reservoir

The following criteria should be met for an optimal Li reservoir to facilitate effective on-demand Li extraction. (1) Li should be stored in a chemically more stable form to minimize chemical corrosion during cycling. Given the low reduction potential of Li/Li^+, it is beneficial to store Li in a phase of elevated potential. (2) Li should not be released during the standard operating voltage window. By decoupling extraction steps with specialized protocols from normal cycling conditions, the reservoir can selectively supplement Li through careful designing of the cycling sequence.

We discovered that Li-Cu alloy would satisfy the criteria based on its unique properties. (1) Li-Cu alloy phase becomes accessible by thermal treatment at a high temperature (>180.6°C) (Figure 1A).[27–30] At room temperature, Li and Cu do not preferably form an alloy electrochemically or chemically owing to slow kinetics, showing hysteretic behavior.[31,32] (2) Reduction potential of the Li-Cu alloy (1.2 V vs. Li/Li^+) is above the normal operating window of anodes.[29] The existence of two-phase regions of face-centered-cubic (FCC)-(Cu) and Li at T > 180.6°C hints at the solubility of Li in a solid solution, overcoming low Li solubility in FCC-(Cu).[33] In addition, a high reduction potential of Li in Li-Cu alloy insinuates lower electrochemical reactivity in this phase, suggesting notable stability for a Li reservoir.

We fabricate Li-Cu alloy foil from commercially available thin Li on Cu foil with good interfacial contact between them. At T > 180.6°C, molten Li diffuses into the Cu potentially through grain boundary (GB) diffusion followed by alloying of grains.[31] Subsequently, Li-Cu alloy foil is introduced into batteries as a prelithiated CC. In a discharge step within a conventional operation window, Li-Cu alloy CC remains electrochemically silent because it has not reached the potential to release Li (step I in Figure 1B). By contrast, during a special discharging protocol in which the anode reaches higher potential (>1.2 V vs. Li/Li^+), the prelithiated CC starts to release additional Li^+, providing extra capacity (step II in Figure 1B). This Li extraction step is accessible selectively by manipulating cycling protocols, allowing on-demand extraction of Li from the Li-Cu CC to rejuvenate battery capacity and extend capacity retention. Furthermore, we demonstrate that Li-Cu alloy CC provides a significant improvement over conventional Cu CC in reversible capacity owing to its capability to selectively extract additional Li (Figure 1C).

Please cite this article in press as: Lee et al., On-demand capacity extraction through thermo-electrochemical hysteresis in metastable Li-Cu alloy, Joule (2026), https://doi.org/10.1016/j.joule.2026.102632

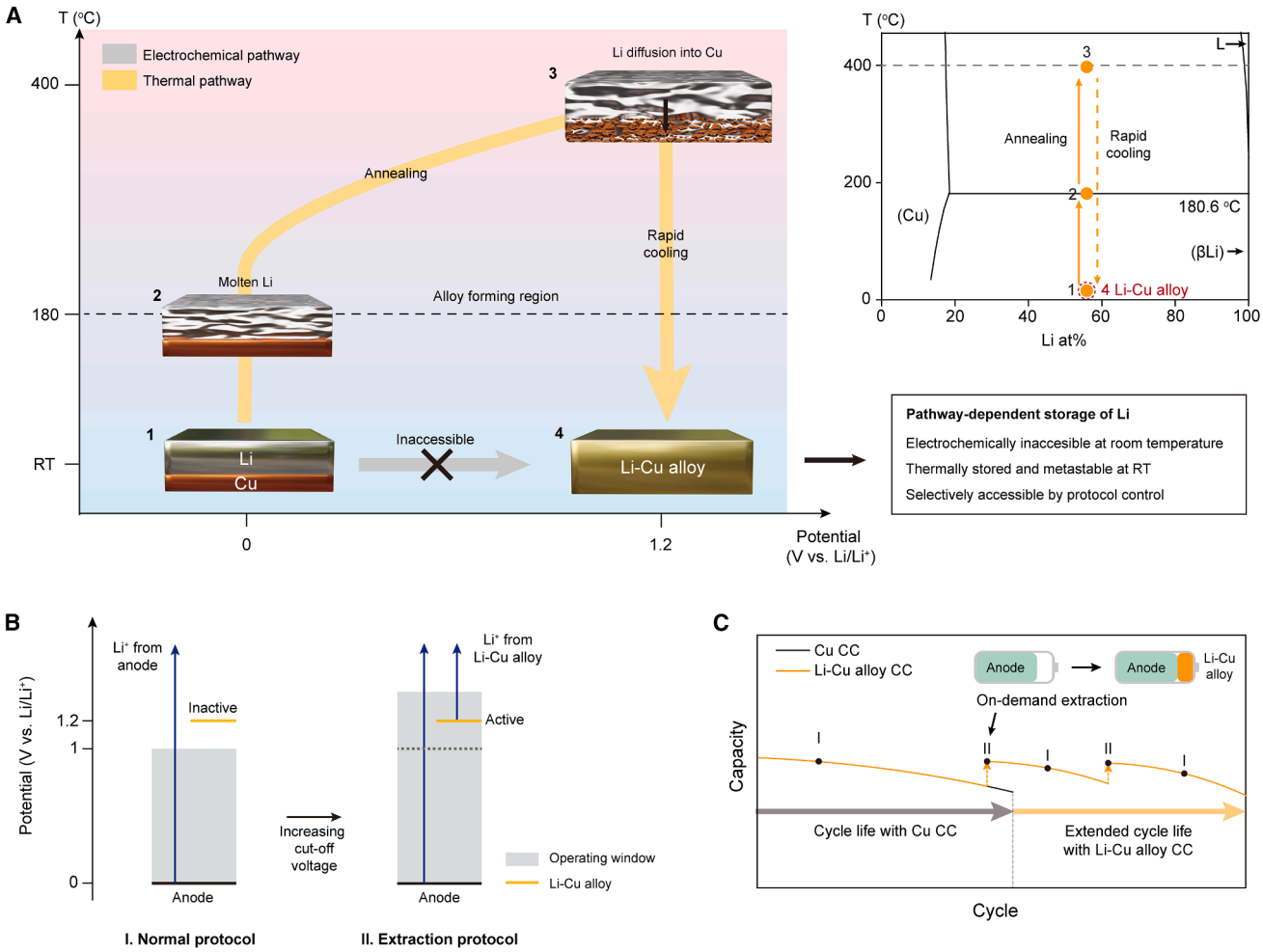

Figure 1. Synthesis pathway of metastable Li-Cu alloy and on-demand capacity extraction

(A) Synthesis pathway of Li-Cu alloy (left) and phase diagram of Li-Cu system (right). (Left) Yellow and gray arrows represent thermal and electrochemical pathways, respectively. (Right) Orange dots correspond to the point in the thermal pathway from the temperature vs. potential plot. Orange line and dashed line represent annealing and rapid cooling steps, respectively. Red dashed dot shows the location of metastable Li-Cu alloy phase after the synthesis. Data extracted from reference Okamoto et al.[27] with permission.

(B) A scheme of operating window (gray) and Li^+ transport (blue arrow) during normal (left) and extraction protocol (right). In the extraction protocol, cutoff voltage of the anode is intentionally increased to include the reduction potential of the Li-Cu alloy (yellow), and Li extraction from the Li-Cu alloy is activated.

(C) Schematic illustrations of the cycle performance of Li batteries with a conventional Cu current collector (CC, black) and Li-Cu alloy CC (orange). Cycles marked with I and II represent normal cycles and extraction cycles from (B), respectively. Multiple on-demand extraction steps (II) lead to significant increase in cycle life with Li-Cu alloy CC.

Fabrication and structural analyses of Li-Cu alloy

To prove our concept, we synthesized the Li-Cu alloy foil by annealing commercial thin Li (20 μm) on Cu foil (11 μm) (Li/Cu foil (Figure S1), Li atom % ~62.3%) in an oven (Ar glove box, 400°C), followed by rapid natural cooling at room temperature. A fixed temperature of 400°C was selected based on the temperature boundaries of the two-phase region between liquid Li and a Cu_xLi phase without intermetallic compounds and used as the reaction condition for all annealing experiments.[33] Rapid cooling step facilitates the alloy phase to remain as a metastable state at room temperature. The time of annealing varied from 0 (pristine) to 0.5, 1, 2, and 3 h, denoted by Li-Cu-0, Li-Cu-0.5, Li-Cu-1, Li-Cu-2, and Li-Cu-3, respectively.

We performed X-ray diffraction (XRD) to confirm the emergence of the Li-Cu alloy phase with thermal annealing (Figures 2A–2C). After 0.5 h of annealing, we observed characteristic peaks of the Li-Cu alloy at $2\theta = 42.9°$, 50°, and 73.4°, corresponding to an FCC unit cell ($a = b = c \sim 3.645$ Å) larger than that of Cu ($a = b = c \sim 3.615$ Å)[29] (Figures 2A and S2). Larger d-spacing of Li-Cu alloy (200) plane (0.182 nm) than Cu (200) plane (0.180 nm) from fast-Fourier transformation (FFT) images of transmission electron microscopy (TEM) cross-validated the isotropic increase of lattice parameters after alloying.[34] (Note S1; Figure S3.) XRD peaks of Li^0 were elusive owing to its low Z and subsequent low sensitivity to X-ray characterization. Furthermore, as the annealing time increased from 0.5 to

Please cite this article in press as: Lee et al., On-demand capacity extraction through thermo-electrochemical hysteresis in metastable Li-Cu alloy, Joule (2026), https://doi.org/10.1016/j.joule.2026.102632

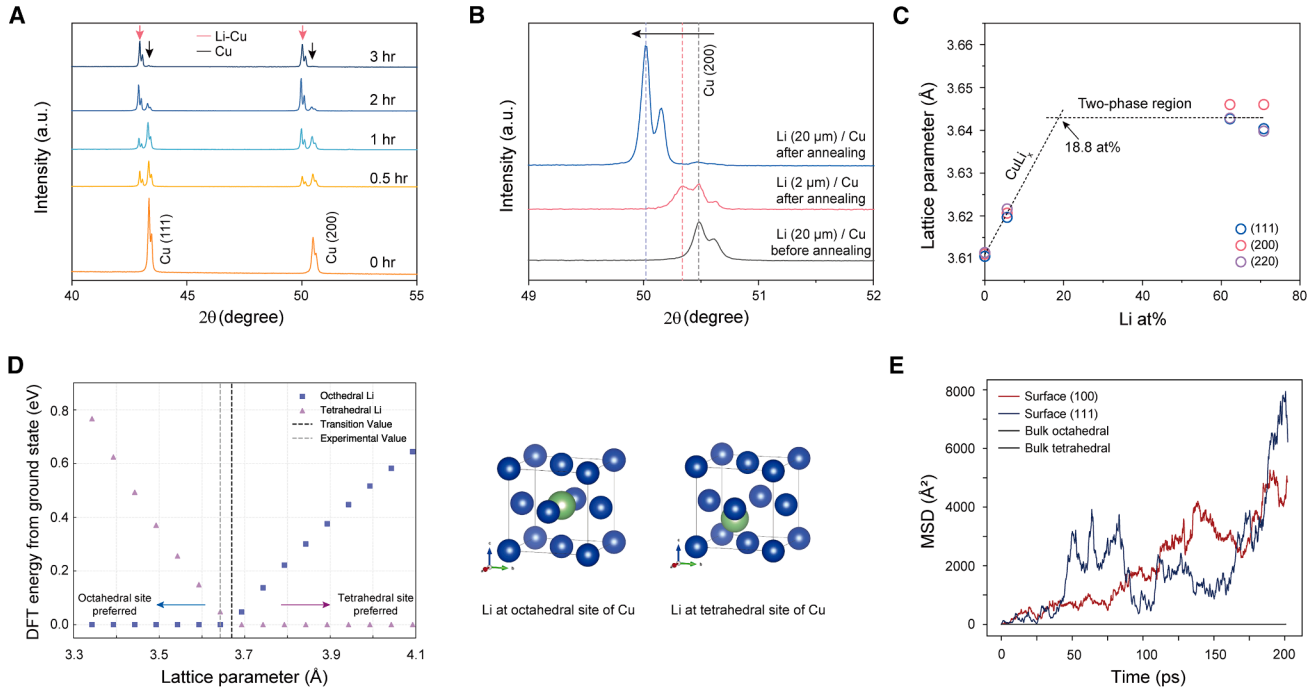

Figure 2. Fabrication of Li-Cu alloy and structural analysis

(A and B) XRD patterns of commercial Li on Cu foil with (A) various annealing times (0, 0.5, 1, 2, and 3 h) and (B) different amounts of Li infused into Cu.

(C) Lattice parameters from XRD peaks of Li-Cu alloy at multiple atom % of Li. Lattice parameters corresponding to Cu (111) (blue), Cu (200) (red), and Cu (220) (purple) are displayed.

(D) DFT energies of Cu unit cells with a Li atom at two different interstitial sites (octahedral [blue] and tetrahedral [purple]). Lattice parameters of each unit cell were varied from 3.3 to 4.1 A.

(E) AIMD-simulated mean square distance (MSD) of Li on each location in Cu lattice. Bulk (octahedral) (gray) and bulk (tetrahedral) (black) refer to lattices with Li located at corresponding sites inside.

3 h, XRD peaks of Li-Cu alloy became dominant over Cu, implying near-complete phase transformation from Cu to $CuLi_x$. Optical images of Li-Cu-1 and Li-Cu-3 support these results based on the transition from gold to dark red color, representing changes in phases over time (Figure S4). On the other hand, thinner Li foil with a smaller atom % of Li (2 μm on 11 μm Cu, Li atom % ~ 5.67%) exhibited smaller peak shifts in XRD, possibly ascribed to insufficient of Li for complete phase transformation. These results confirmed the successful synthesis of a Li-Cu alloy with the annealing process and its dependence on time and initial Li atom %.

To delve deeper into the structural analyses of the Li-Cu alloy, we utilized a parametric method on the $CuLi_x$ phase (Note S2).[35] Lattice parameters of various Li-Cu samples (Li atom % = 0, 5.7, 62.2, and 70.8%) derived from Bragg's law show a typical trend of a two-phase region and the intersection of two extrapolated lines at ~18.8 atom % Li, close to the location of the solvus line (~20 atom % Li) at 400°C. With a similar result from Pawley refinements (Figures S5 and S6; Table S1), we conjecture that the atomic ratio of Cu and Li is close to 4 at the boundary of the $CuLi_x$ phase, or Cu_4Li, matching the phase diagram.[33]

Density functional theory (DFT) simulations for Cu_4Li unit cells were conducted to better understand its crystal structure (Figure 2D). We constructed FCC unit cells of Cu with a Li atom at an octahedral site (Cu_4Li(octa)) or a tetrahedral site (Cu_4Li(tetra)) (Figure S7). A configuration consisting of a Li atom sitting at a Cu site with the Cu atom in an interstitial site showed significantly higher energy or was unable to converge in its forces and thus was not considered as a possible unit cell. DFT energy calculations with lattice parameters as variables in Figure 2D exhibit that Cu_4Li(octa) are preferred for the lattice parameter (a = b = c = 3.645 Å) from experiments, as supported by simulated powder XRD spectra of possible unit cells (Figure S8). Thus, in the unit cell of Cu_4Li, a Li atom occupies an interstitial site in the Cu unit cell.

We further used *ab initio* molecular dynamics (AIMD) simulations to investigate the alloying reaction above the T_m of Li. Diffusion of Li in a liquid state is a poorly understood phenomenon due to its high reactivity, and the mechanism of the alloying reaction remains unexplored. From a series of model systems with exposed (111) and (100) surfaces at 700 K, we observed that the mean squared distances (MSDs) of Li on faceted surfaces were much higher than that of Li in bulk Cu, exhibiting higher Li diffusivity via grain boundaries than through grains (Figures 2E and S9; Videos S1, S2, S3, and S4). This was in accordance with previous reports that Li diffusion is much faster through GB,[31,36] which might be attributed to fewer neighboring Cu atoms and thus lower activation energy for diffusion. The result was also consistent with morphological changes observed in scanning electron microscopy (SEM) over different stages of

Please cite this article in press as: Lee et al., On-demand capacity extraction through thermo-electrochemical hysteresis in metastable Li-Cu alloy, Joule (2026), https://doi.org/10.1016/j.joule.2026.102632

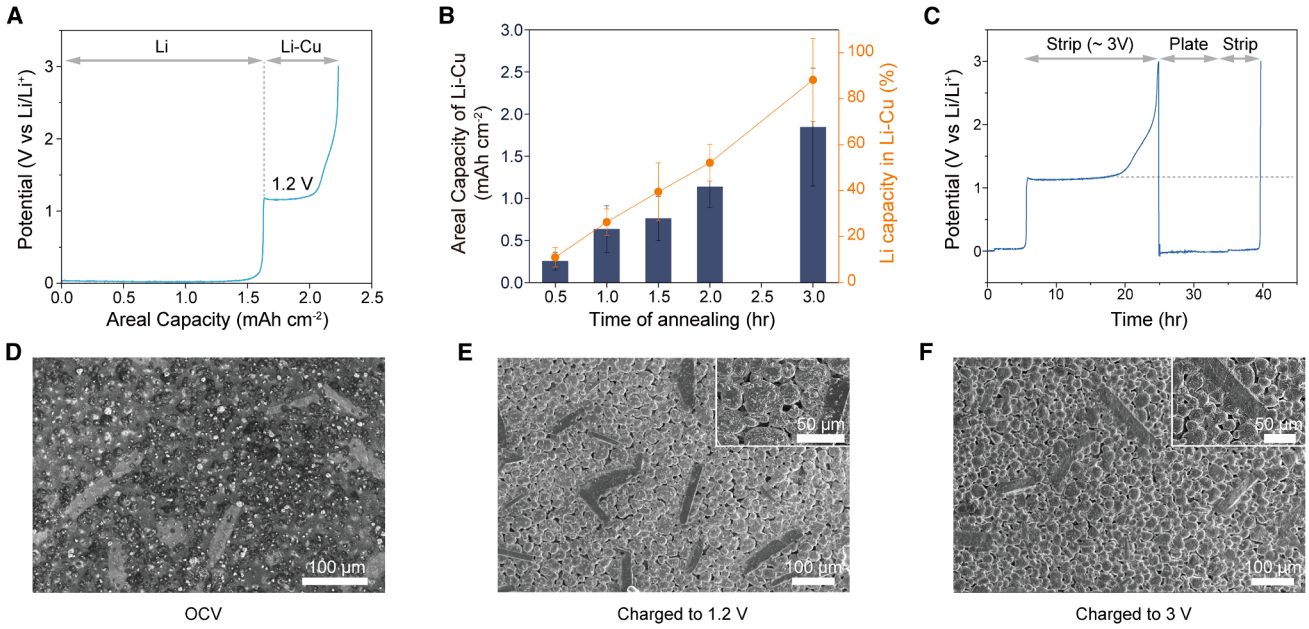

Figure 3. Electrochemical characterizations of Li-Cu alloy

(A) Voltage profile of 1 h annealed Li-Cu alloy under Li stripping in 1 M LiTFSI DOL/DME (1:1 v/v) 5% $LiNO_3$ electrolyte.

(B) Areal capacity of Li stored in Li-Cu alloy samples (blue) and its percentage out of the total amount of Li after annealing. Annealing time was varied from 0.5 to 3 h.

(C) Plating and stripping behavior of Li-Cu alloy after Li extraction. 1 mAh cm^{-2} of Li was deposited following the initial stripping step up to 3 V and stripped again to 1 V.

(D–F) Top-view SEM images of Li-Cu alloy samples at OCV, 1.2 V, and 3 V, respectively.

annealing, in which molten Li diffused rapidly into the Cu foil through GB, succeeded by wetting on a lithiophilic surface (Li-Cu alloy),[29] and bulk alloying of Cu grains (Figure S10).

Electrochemical properties of Li-Cu alloy

To verify the capability of the Li-Cu alloy as a Li reservoir, we investigated its electrochemical characteristics in Li||Li-Cu alloy coin cell configurations with 1 M lithium bis(trifluoromethane)sulfonimide (LiTFSI) 1,3-dioxolane (DOL)/1,2-dimethoxyethane (DME) (1:1 v/v) + 5% $LiNO_3$ (DDN) electrolyte (Figure 3). From the voltage profile of the Li||Li-Cu-1 cell during charging at 0.1 mA cm^{-2} (Figure 3A), two distinctive Li stripping behaviors were observed: (1) 1.6 mAh cm^{-2} of Li^0 stripping around 0 V (vs. Li/Li^+), and (2) 0.7 mAh cm^{-2} of Li extraction from Li-Cu alloy at 1.2 V. Based on the reduction potential and the plateau-shaped voltage profile, it was apparent that Li in Li-Cu-1 was electrochemically released via the phase transformation within a two-phase region. Moreover, the elongation of the plateau at 1.2 V highly depended on annealing time (Figures 3B and S11), attributing to the temporal evolution of the Li-Cu alloy phase (Figure 2A). It was noteworthy that the areal capacity could be controlled from 0.2 to ~2 mAh cm^{-2} by tuning the percentage of Li-Cu alloy formed. Our samples had a significantly higher capacity of 1 mAh cm^{-2} (~629 mAh g^{-1}) than the previously reported Li-Cu alloy (<16 mAh g^{-1}) because we did not include water exposure steps.[29] Same experiments in various electrolytes revealed similar voltage profiles and capacities, suggesting that the stored capacities did not largely depend on the type of electrolytes used (Figure S12). Notably, the characteristic plateau at 1.2 V was not present after the first extraction, both upon plating and stripping of Li on the CC (Figure 3C). This indicated that once Li was extracted from the Li-Cu alloy, it could no longer access the Li-Cu alloy phase electrochemically at room temperature, representing the potential of the phase as a release-only reservoir. This result is noteworthy because it provides key evidence of thermo-electrochemical hysteresis in Li-Cu alloy. The presence of Li on Li-Cu alloy from SEM and XRD results after a strip-plate process supported our analysis of voltage curves (Figures S13 and S14). This was particularly important because it emphasizes the role of the Li-Cu alloy both as a Li reservoir during an extraction step and as an inactive Li reservoir otherwise.

The correlation of electrochemical properties to morphological aspects of Li-Cu alloy was described by microscopic techniques (Figures 3D–3F). From the SEM image, we observed that the as-prepared Li-Cu-2 has a flat morphology with the presence of microstructures such as microparticles (Figure 3D). After charging a Li||Li-Cu-2 cell to 1.2 V, gaps between microparticles (~25 μm) became visible (Figure 3E). According to the report,[29] we speculated that microstructures corresponded to Li-Cu alloy, while metallic Li filled in the gaps. Interestingly, image analysis on Figures 3E and 3F showed that the microstructure remained after further charging to 3 V (average particle size from 16.3 to 16.4 μm and pore area fraction from 64% to 67%), an indication that the extraction of Li has minimal impact on the overall morphology of particles. We observed matching results from Li-Cu-3, implying that this trend is not limited to Li-Cu alloy with lower capacity (Figure S15). A similar conclusion could be

Please cite this article in press as: Lee et al., On-demand capacity extraction through thermo-electrochemical hysteresis in metastable Li-Cu alloy, Joule (2026), https://doi.org/10.1016/j.joule.2026.102632

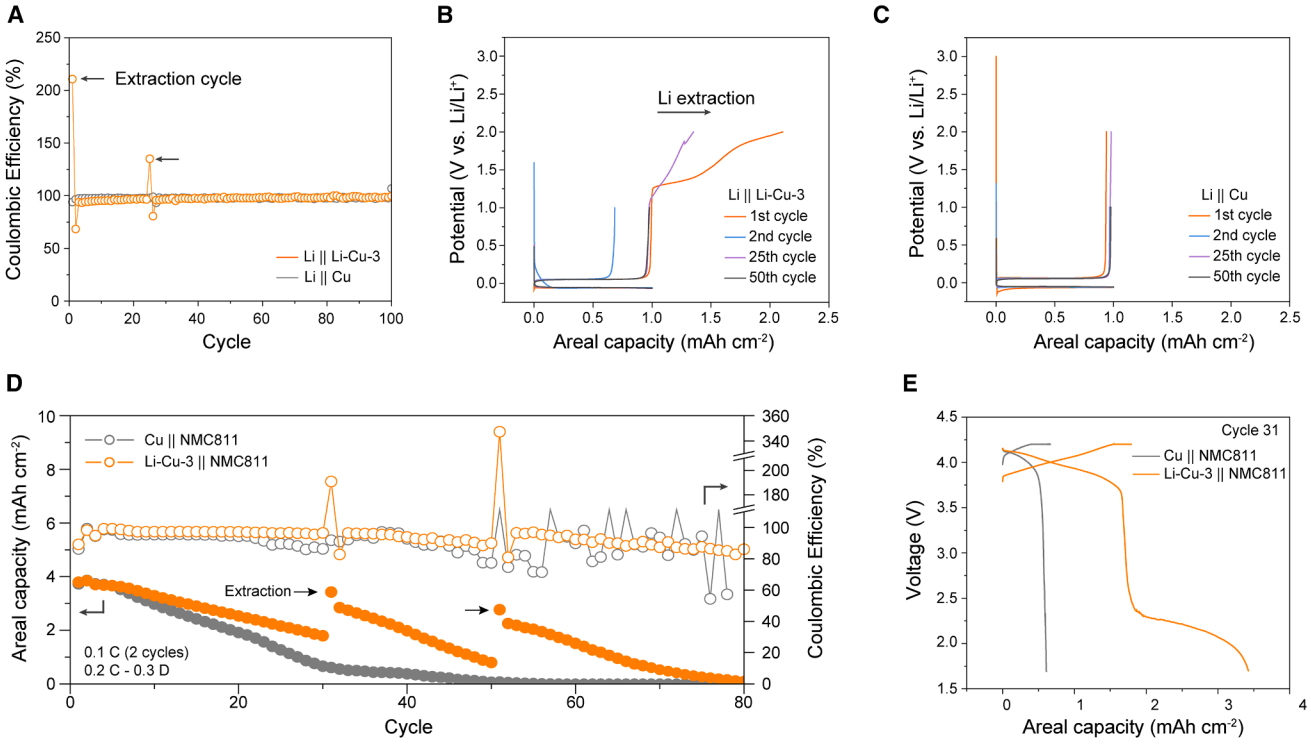

Figure 4. Li-Cu alloy enables improved ICE for anodes

(A–C) (A) Representative half-cell cycling profiles of Li||Cu (gray) and Li-Cu alloy (Li||Li-Cu alloy, orange) CC. Li extraction steps were conducted on the 1st and the 25th cycles (marked with arrows). The cycling was performed at 1 mA cm^{-2} for 1 mAh cm^{-2}. Charge-discharge voltage profiles of Li||Li-Cu alloy (B) and Li||Cu cells (C) at 1st (orange), 2nd (blue), 25th (purple), and 50th (gray) cycles.

(D) Representative cycling profiles of anode-free Cu||NMC811 (gray) and Li-Cu-3||NMC811 (orange) with LPF electrolyte. Cells were cycled at 0.1C (2 cycles) followed by a CCCV protocol (0.2 C charging—CV at 4.2 V down to 0.05C–0.3C discharging). Discharge areal capacity (filled circle) and CE (open circle) are shown in the figure. Li was extracted from CC at the 31st and 51st cycles.

(E) Corresponding voltage profiles of Cu||NMC811 (gray) and Li-Cu-3||NMC811 (orange) at the 31st cycle.

drawn by comparing XRD spectra and optical microscopy (OM) images of the alloy before (1.2 V) and after the extraction process (3 V) (Figures S16–S19; Video S5).[37] Thus, we believe that the Li-Cu alloy would keep its morphology during the extraction step, confirming the morphological stability as a CC.

We employed X-ray photoelectron spectroscopy (XPS) to assess the chemical stability of Li-Cu alloy in electrolyte. Both Li 1s and O 1s spectra represented the presence of Li_2O prior to the exposure to the electrolyte (Figure S20). After resting Li||Li, Li||Li-Cu-2, and Li-Cu-2||Li-Cu-2 cells for 24 h in 1 M $LiPF_6$ in ethylene carbonate (EC)/diethyl carbonate (DEC) (1:1 v/v) + 10% fluoroethylene carbonate (FEC) electrolyte (LPF electrolyte), high-resolution XPS spectra of F 1s and O 1s showed the higher area % of Li-F and C-F in Li-Cu-2 surfaces than those of Li, referring to the formation of more F-rich SEI on the Li-Cu alloy (Figures S21 and S22). A similar trend—more F-rich SEI on Li-Cu alloy—was obtained after forming SEI on Cu and Li-Cu alloy (Figure S23). Higher ratio of LiF in the SEI on Li-Cu alloy attributed to the Li^+-coordinated FEC-driven SEI than EC clusters or uncoordinated FEC molecules at 1.2 V.[38] Consequently, Li-Cu alloy is more favorable to form a beneficial F-rich SEI ascribed to its higher reduction potential than Li in LPF.

Overall, notable features of the Li-Cu alloy were revealed by structural, electrochemical, and microscopic analysis: (1) the two-phase region of Cu_4Li and a Li could electrochemically store Li at 1.2 V vs. Li/Li^+ (Figures 3A and 3B). (2) Upon annealing, Li diffused mostly through grain boundaries of Cu (Extended Figure 1). (3) Once stripped, Li could not go into Cu lattices again to reform Li-Cu electrochemically (Figure 3C). (4) There were minimal morphological changes on microstructures during the extraction process from Li-Cu (Figures 3D–3I).

On-demand extraction in LMBs

To confirm the feasibility of Li-Cu alloy as a prelithiated CC, we first applied Li-Cu alloy in LMBs to supplement for continuous capacity loss (Figure 4). Li||Li-Cu CC half cells were cycled with a localized high concentration (LHCE) electrolyte (LiFSI [lithium bis(fluorosulfonyl)imide]-1.2DME-3TTE [tetrafluoroethyl-2,2,3,3-tetrafluoropropyl ether]). Li-Cu-3 was selected as CC to utilize its large amount of stored capacity (~2 mA cm^{-2}) in the following experiments. We placed "extraction cycles" at the 1st and the 25th cycles, in which cells were charged to 2 V, enabling extraction of Li from CCs. In these extraction cycles, Li||Li-Cu-3 exhibited extraordinary Coulombic efficiency (CE) of 210% and 135% in the 1st and 25th cycles, respectively, by virtue of

Please cite this article in press as: Lee et al., On-demand capacity extraction through thermo-electrochemical hysteresis in metastable Li-Cu alloy, Joule (2026), https://doi.org/10.1016/j.joule.2026.102632

additional Li supplied from Li-Cu CC (Figure 4A). By contrast, the Li||Cu cell showed 90% and 99% CE in the 1st and 25th cycles, respectively, with the same protocol. Improved CE in the 25th cycle demonstrated that the capacity boost from Li-Cu CC not only enhanced the CE of the initial cycle but also in the later cycle, implying the capability of Li-Cu to store and release Li during cycling.

We validated the Li storage and release capability of Li-Cu CC with voltage profiles and electrochemical impedance spectroscopy (EIS). Voltage profiles of Li-Cu CC showed the extraction curves starting at 1.2 V in the 1st and the 25th cycles, while no additional peaks were visible from Cu CC (Figures 4B and 4C). Moreover, nucleation overpotential at the 1st discharging sequence for Li-Cu CC (~79 mV) was lower than Cu CC (~147 mV), owing to the lithiophilic nature of Li-Cu alloy. At the 25th cycle, less Li is extracted from the Li-Cu alloy (135% CE) than in the 1st cycle due to the already utilized amount of Li in the 1st cycle. In addition, EIS results after 24 h of rest also proved the Li-reserving capability of the Li-Cu alloy because there was minimal corrosion even in the carbonate electrolyte (Figure S24). Based on these results, we believe that (1) the extraction step can be placed in any cycle, e.g., the 25th cycle, enabling "on-demand Li extraction," and (2) multiple extraction cycles are feasible by controlling the amount of Li capacity extracted in each cycle, functioning as an optimal reservoir.

The Li-Cu CC was further integrated into pseudo-anode-free cells paired with NMC811 cathodes to assess its role in capacity retention enhancement. A custom cycling protocol was designed with two Li extraction cycles at the 31st and 51st cycles, targeting both "on demand" and "multiple" Li extraction from the CC. The lower cutoff voltage of cycle 31 was set to be 1.7 V, whereas that of cycle 51 was 1.5 V to control the degree of extraction in multiple steps. Cu||NMC811 and Li-Cu-3||NMC811 (4 mAh cm^{-2}) cells assembled in LPF electrolyte were cycled with the same protocol—two activation cycles (0.1C) and followed by constant current-constant voltage (CCCV) protocols at 0.2C (constant current [0.2C] to 4.2 V, constant voltage to 0.05C, and discharge at 0.3C to 3 V). Except for the extraction steps, all parameters remained constant. Notably, Li-Cu-3||NMC811 exhibited higher capacity than Cu||NMC811 after 5 cycles, owing to both the F-rich nature of the SEI formed on the Li-Cu and higher lithiophilicity (Figure 4D).

During the extraction cycles, Li-Cu-3||NMC811 showed substantial capacity enhancement: 1.64 mAh cm^{-2} (cycle 31) and 1.97 mAh cm^{-2} (cycle 51) of Li were extracted from Li-Cu-3, achieving 200% and 350% CE, respectively (Figures S25 and S26). Despite partial loss in the subsequent cycles, significant amounts of recovered capacities prolonged the cycle life up to 66 cycles (>0.7 mAh cm^{-2})—more than twice that from Cu||NMC811 cells, which did not show any noticeable boost in capacities from extraction cycles in the same protocol (Figure S27). In addition, we repeated the same experiments with LHCE electrolyte to confirm the general applicability of Li-Cu CC to various electrolytes (Figure S28).[10] Analogous to results with LPF electrolyte, we could extract Li in multiple steps only from Li-Cu CC (Figures S29 and S30). The approach sustained 2.5 mAh cm^{-2} longer in Li-Cu-3||NMC811 cells (57 cycles) than in Cu||NMC811 cells (40 cycles) (Figure S31) by 1.4-fold. These results emphasized the utility of Li-Cu CC as a prelithiated CC with on-demand Li extraction capability. Through thoughtful protocol design, Li-Cu CC can supplement capacity loss at desired cycles for better managing cycle life in LMBs.

Li extraction in activation cycles of LIBs

To evaluate the practical applicability of prelithiated Cu CCs, we assembled Li||Gr half-cell configurations in LPF electrolyte (Figures 5A–5C). In particular, freestanding Gr electrodes (Gr, 300 mAh g^{-1}) were paired with the Li-Cu alloy (Gr + Li-Cu) to verify the capability to prelithiate and support Gr anodes (Figure S32).[39] Li-Cu-2 (~1.1 mAh cm^{-2}) was chosen to match the Li loss for Gr electrodes in the 1st cycle (~0.83 mAh cm^{-2}) (Figure S33). The decreased OCV (~1.26 V) and increased initial discharge capacity (~364 mAh g^{-1}) of Li||Gr + Li-Cu-2 from Li||Gr (~2.71 V and ~331 mAh g^{-1}, respectively) might be attributed to remaining Li on the surface of Li-Cu-2 (Figure 5A). Upon charging from 50 mV to 3 V (vs. Li/Li^+), a distinct peak at 1.2 V was exclusively observed in the Li||Gr + Li-Cu-2 cell, accompanied by an additional capacity (40 mAh g^{-1}). This enabled an improved ICE of ~98%, substantially higher than the Li||Gr cell (CE ~ 82%). In continuous cycling at 0.05C, Li||Gr + Li-Cu-2 also showed superior ICE with stable cyclability, demonstrating both the directional Li extraction and feasibility as a CC of Li-Cu-2 (Figures 5B and S34). Furthermore, the degree of lithiation on Gr anodes could be tuned with Li-Cu CCs (Figure 5C). By modulating the prelithiated amount in CC from 0 mAh cm^{-2} (no CC) to 1.8 mAh cm^{-2} (Li-Cu-3), the corresponding ICE changed from 80.6% to 106.8%. Back-calculated supplements from the Li-Cu CC yielded 0.64, 1.02, and 1.37 mAh cm^{-2} from Li-Cu-1, Li-Cu-2, and Li-Cu-3, respectively, aligning with the experimentally measured capacities (Figure 3B). These findings demonstrated that our Li-Cu CC could effectively compensate for the initial capacity loss in LIBs.

We further extended our approach of prelithiated CC and on-demand Li extraction to Gr||NMC811 full cells (Figures 5D–5G). To confirm that selective lithiation is feasible in LIBs, we prepared Cu + Gr||NMC 811 and Li-Cu-3 + Gr||NMC 811 full cells in LPF electrolyte. Cells were cycled at 0.1C during activation cycles (3 cycles) and followed by cycles at 0.5C. The extraction step was designed as a discharge step with the lower cutoff voltage of 1.5 V, accounting for the reduction potential of the Li-Cu alloy. With the extraction step in the first cycle (E1), Li-Cu-3 + Gr||NMC811 cells (Li-Cu-E1) exhibited an ICE of 82.5%, significantly higher than Cu + Gr||NMC811 (Cu-E1, 55.4%). The distinct peak observed at ~2 V indicated the full cell voltage of initial Li release, while it was not visible from Cu CC (Figure S35). The substantial increase in 1st cycle CE led to significantly enhanced capacity in the following cycles. Furthermore, we confirmed that the extraction step in the second cycle (E2) could also improve the 2nd cycle CE from 84.8% (Cu + Gr||NMC811, Cu-E2) to 118.7% (Li-Cu-3 + Gr||NMC811, Li-Cu-E2) (Figure S36). The result indicated that the on-demand Li extraction was feasible in LIBs as well, supported by a similar amount of retrieved capacity in the E1 protocol (0.4 mAh cm^{-2}) and E2 protocol (0.44 mAh cm^{-2}) (Figures 5E and 5F). However, the cells cycled with the E1 protocol (1.37 mAh cm^{-2}) exhibited 50% higher capacity than cells with the E2 protocol

Please cite this article in press as: Lee et al., On-demand capacity extraction through thermo-electrochemical hysteresis in metastable Li-Cu alloy, Joule (2026), https://doi.org/10.1016/j.joule.2026.102632

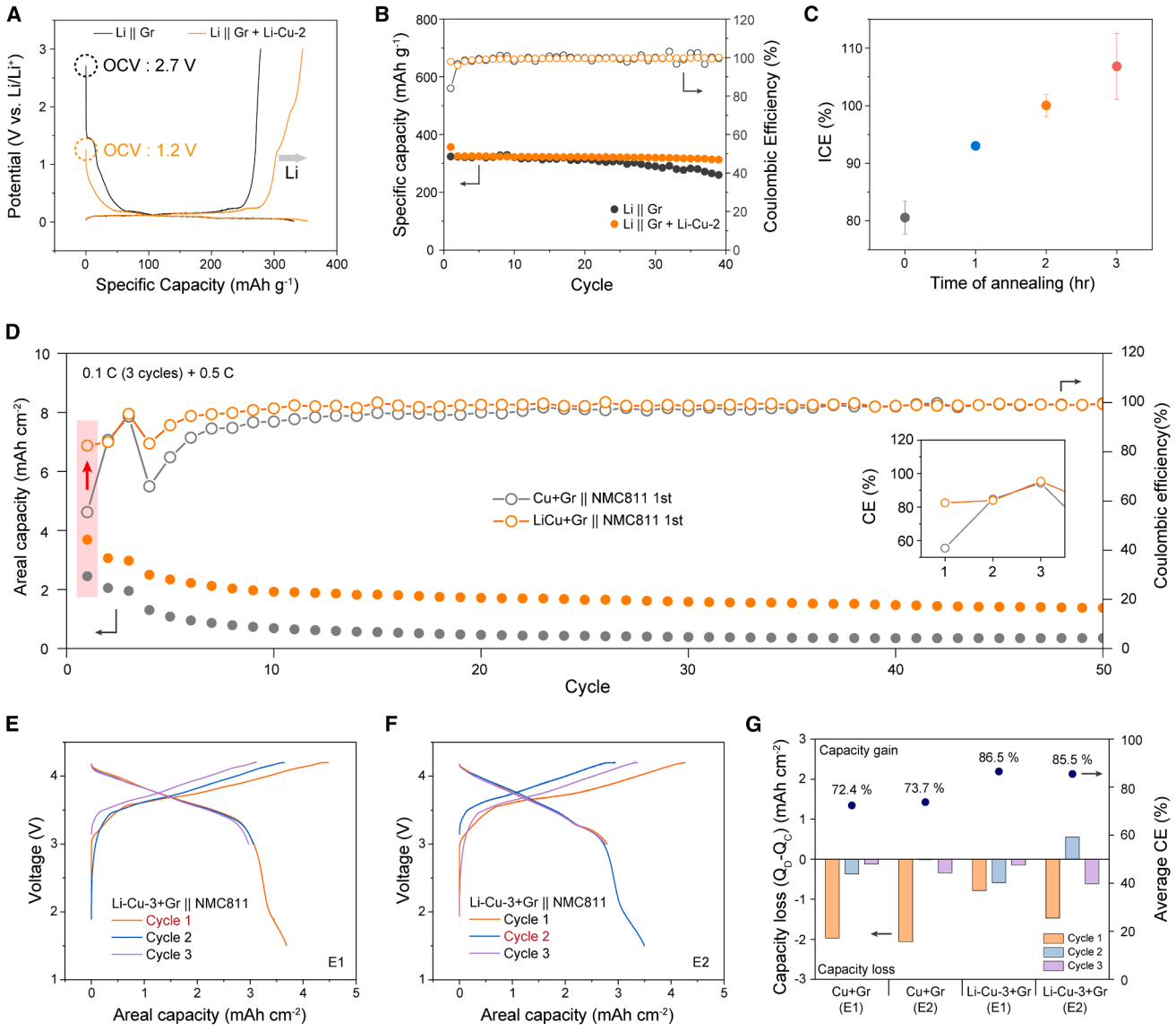

Figure 5. Li-Cu alloy enhances ICE and exhibits higher capacity in full cells

(A) Representative charge-discharge voltage profiles of the Li||Gr (gray) and Li||Gr + Li-Cu (orange) electrodes between 0.01 and 3 V at 0.05C for the initial cycle. Li||Gr + Li-Cu exhibits lower OCV and larger discharge capacity.

(B) Corresponding half-cell cycling profiles of the discharge capacity (filled symbols) and CE (open symbols) at 0.05C.

(C) ICE of bare Gr anodes (depicted as 0 h, gray) and Gr anodes with 1 (blue), 2 (orange), and 3 h (red) annealed Li-Cu alloy CC.

(D–F) (D) Representative cycling profiles of the CE (open circle) and the discharge areal capacity (filled circle) for Cu + Gr||NMC811 and Li-Cu-3 + Gr||NMC811 full cells with the extraction steps on the 1st cycles (E1). The cycling was performed at 0.1C (3 cycles) and followed by 0.5C. First 3-cycle voltage profiles of Li-Cu-3 + Gr||NMC811 full cells with the extraction step in the 1st cycle (E) and the 2nd cycle (F). Extraction cycles are marked in red.

(G) Capacity loss ($Q_D - Q_C$) of cycle 1 (orange), 2 (blue), and 3 (purple) in all types of cells. Average CE of first 3 cycles is shown as navy circles.

(0.9 mAh cm^{-2}) at the 50th cycle, suggesting the benefit of supplementary capacity in the 1st cycle. To get an insight on optimal Li release during activation cycles, we plot the capacity loss, (discharge capacity, Q_D) − (charge capacity, Q_C) of each cycle in Figure 5G. The figure demonstrates the impact of lithiation by showing decreased capacity loss of cells and increased average CE during activation cycles with the Li-Cu CC. In particular, average CE was the highest for Li-Cu-E1, and thus it was critical to supplement Li loss during the first activation cycle for LIBs. Based on these results, we have achieved employment of the Li-Cu CC in LIBs and lithiation in the activation stage for enhanced battery capacity with an insight to optimize the performance.

While the present work establishes the metastable Li-Cu alloy as a functional on-demand Li reservoir, several aspects remain to be addressed for practical implementation. First, the

Please cite this article in press as: Lee et al., On-demand capacity extraction through thermo-electrochemical hysteresis in metastable Li-Cu alloy, Joule (2026), https://doi.org/10.1016/j.joule.2026.102632

as-synthesized porous and microparticulate morphology of the alloy increases the surface area available for SEI formation and can transiently affect the CE. Further optimization of the alloy morphology—for example, through additional annealing to reduce porosity—is expected to mitigate this effect. Second, the integration of the Li-Cu CC with the active electrode requires further development. Moving from the freestanding Gr used in this study and adopting a dry-coating process to form a more intact, mechanically robust electrode directly on the Li-Cu collector represents a promising route toward better interfacial contact and improved cell performance. Finally, although the elevated reduction potential of the Li-Cu alloy confers greater chemical stability than metallic Li, its detailed reactivity toward atmospheric components (H_2O, O_2, and N_2) and its compatibility with conventional slurry-coating processes remain to be systematically evaluated. A dedicated study of the air and dry-air stability of the alloy will be important for assessing its manufacturability. Addressing these aspects will further advance the metastable alloy CC toward practical, high-energy-density battery systems.

Conclusions

In this study, we demonstrate that the metastable phase of a Li alloy can be utilized as a selective Li reservoir. Thermally accessible Li-Cu alloy phase enables controllable prelithiation to mitigate capacity loss in Li batteries. Upon thermal annealing, molten Li rapidly diffuses through Cu foil via grain boundaries driven by faster kinetics for diffusion on Cu facets (100) and (111), followed by bulk diffusion to form a stable two-phase alloy of Cu_4Li and Li. This phase provided a controllable amount of Li capacity with enhanced electrochemical stability. Importantly, the Li stored in the alloy phase is electrochemically accessible only at elevated anode potentials beyond conventional operation windows, enabling protocol-controlled release. As a proof of concept, we integrated the alloy into various configurations of Li batteries and observed the increase in CE with extraction from Li-Cu CC. Furthermore, this type of CC allowed stepwise, on-demand Li extraction during cycling for longer cycle life and enhanced cell capacity. Hence, the Li-Cu alloy can potentially serve both as a CC and a Li reservoir to enhance battery capacity retention. Our approach provides fundamental insights into thermo-electrochemical hysteresis for designing advanced Li-storage materials to enable on-demand rejuvenation of energy-storage devices. By exploring metastable states via thermal pathways, this work expands the library of candidate materials and architectures for high-energy batteries with longer cycle life.

METHODS

Materials

All electrolytes were prepared and handled in an Ar-filled glove box with O_2 level < 0.2 ppm and H_2O level < 0.01 ppm. The DDN electrolyte was prepared by dissolving 1 M LiTFSI (Solvay) in DOL/DME (1:1 v/v) (Sigma-Aldrich) with 5 wt % of $LiNO_3$ (Sigma-Aldrich). The LPF electrolyte was prepared by mixing 1 M $LiPF_6$ in EC/DEC (1:1 v/v) (Gotion) with 10 vol % of FEC (BASF). The LHCE electrolyte was prepared with LiFSI (Fluolyte), DME (Sigma-Alrich), and TTE (SynQuest) in the molar ratio of 1:1.2:3. High-purity Li foil (500 μm, 99.9%, MSE Supplies), Cu foil (12 μm Pred Materials), Celgard 2325 separator (25 μm), and NMC811 (Targray, 4 mAh cm^{-2}) were used to make 2032-type coin cells.

Synthesis of Li-Cu alloy

All synthesis was conducted in an Ar-filled glove box with O_2 level < 0.2 ppm and H_2O level < 0.01 ppm. High-purity thin Li foil (Li/Cu = 20 μm/11 μ, 40 μm/11 μm, 2 μm/18 μm, MSE Supplies) was used to synthesize Li-Cu alloy. Before annealing, both sides of the foils were scraped to remove contamination or oxide layers. All foils were placed on a stainless-steel tray and annealed at 400°C for 0.5, 1, 2, and 3 h in the pre-heated oven. Samples were taken out of the oven for natural cooling to room temperature. The prepared Li-Cu alloy was punched for further experiments.

Synthesis of freestanding Gr electrode

Freestanding Gr anode was prepared with a standard slurry-coating process. All powders were dried in the oven before use to remove water contamination. Gr powder (MTI), Super P conductive carbon black, carbon nanotube (Tuball), and polyvinylidene fluoride (PVDF, Tuball) were mixed in the weight ratio of 86:2:2:10 for slurry preparation, with *N*-methyl-2-pyrrolidone (Alfa Aeser) as solvent. The Gr slurry was evenly mixed with a thinky mixer and coated on polyester (PET)-coated aluminum (Al) films by doctor blading. The coated slurry was dried in a vacuum oven for 2 days to completely dry the solvent. After drying, the Gr electrode was peeled off from the PET-coated Al films and calendared for further use. Fabricated Gr electrodes had a specific capacity of ~300 mAh g^{-1} and an areal capacity of 5.2 mAh cm^{-2}.

Characterizations

All samples were prepared and sealed inside an Ar-filled glove box to prevent air exposure. XRD patterns were measured on a PANalytical Empyrean with Cu Kα (8.04 eV) as the X-ray source and X-ray tube working power of 45 kV/40 mA. Both Bragg's law and Pawley refinement were used to analyze lattice constants. SEM images were collected using a Thermo Fisher Scientific Apreo S LoVac scanning electron microscope. Cross-sectional images were taken by tearing samples and mounting them on SEM holders. For XPS measurement of disassembled cells, surfaces of Li of Li-Cu alloy were rinsed with 50 μL of corresponding pure solvents of electrolytes (DEC for LPF and DME for ether-based electrolytes) and dried in an Ar environment. Vacuum transfer vessels were used to transfer samples to an XPS chamber. XPS measurements were conducted on a PHI Versaprobe IV using a monochromatic Al Kα source. For experiments on forming SEI on Cu or Li-Cu alloy, SEI was formed on Cu and Li-Cu alloy using a CCCV protocol using LPF electrolyte. The discharging current was applied at 50 μA cm^{-2} until the voltage reached 10 mV vs. Li/Li^+. The voltage was held at this level until the current dropped below 10 μA cm^{-2}. Cells were disassembled in an Ar-filled glovebox with O_2 concentration below 0.2 ppm and H_2O concentration below 0.01 ppm. The electrodes were rinsed with 15 μL of DEC (Sigma) three times to remove residual electrolyte salts, then transferred to an XPS chamber using a vacuum

transfer vessel. For analysis, the C 1s peak at 284.5 eV was set as the reference for spectral shifting using MultiPak software. For TEM analysis, Li-Cu alloy samples were transferred to lacey carbon-supported copper grids and water treated to remove residual Li. Details on sample preparation for TEM are explained in Note S1. TEM images were taken with an FEI Titan 80-300 environmental TEM at an acceleration voltage of 300 kV. All FFT indexing measurements were divided by the correction factor of 0.94 to compensate for a calibration offset. Modified coin cell assembly for *operando* OM was carried out in accordance with a previous report. Olympus BX51 optical microscope and Swiftcam SC1803 were used to record time-lapse optical images.

DFT simulations

DFT calculations were done in the Vienna ab initio simulation package (VASP),[40] within the projector augmented wave (PAW) formalism.[41] Since we expected a conductive phase, calculations were done with the generalized gradient approximations (GGAs) exchange-correlation functional of Perdew-Burke-Ernzerhof (PBE)[42] with no Hubbard correction on copper. A gamma-centered grid of 21 × 21 × 21, a plane wave cutoff of 520 eV, and a Gaussian smearing of 0.2 eV were used for the calculations. Atomic positions were relaxed to a 1E-6 eV/Å convergence criterion at different lattice parameters for the octahedral and tetrahedral Li interstitial sites in an FCC copper unit cell (totaling 5 atoms in the atomic cell). AIMD calculations were performed at 700 K, using a Nosé-Hoover thermostat and a timestep of 0.2 fs. A 1 × 1 × 1 gamma-centered grid was used, with the same electronic convergence criteria, exchange-correlation functionals, and pseudopotentials as the ionic relaxation calculations.

Electrochemistry

2032-type coin cells were prepared for electrochemical experiments. LPF, DDN, and LHCE electrolytes were used in this study. Li||Gr and Li||Gr + Li-Cu-2 coin cells with 50 μL of LPF electrolyte were prepared and cycled from 0.05 to 3 V at 0.05C. All Li-Cu alloy samples were pre-stripped to 1.1 V at 0.1 mA cm^{-2} to remove residual metallic Li and transferred to new coin cells, predominantly utilizing the capacity from the alloyed phases. For Li||Li-Cu and Li||Cu half cells, 40 μL of LHCE electrolytes were used, and 50 μL of specified electrolytes were used in all other cases. All cells were rested for at least 1 h after fabrication for sufficient wetting. For Gr-based coin cells with Li-Cu CC, Gr electrodes (~21.64 mg) were placed on Li-Cu CC, and pressure was applied for better contact. EIS was carried out with Biologics VMP3 with the frequency range from 1 MHz to 100 mHz. All cycling experiments were performed using LAND cycling instruments. Capacity measurements of Li-Cu alloy were performed with Li||Li-Cu coin cells and charged to 3 V (vs. Li/Li^+) at a CC of 0.1 mA cm^{-2}. Li||Gr and Li||Gr + Li-Cu cells were cycled at 0.05C with a voltage window of 0.05–3 V vs. Li/Li^+. Li||Cu and Li||Li-Cu were cycled at a CC of 1 mA cm^{-2} to 1 mAh cm^{-2} during discharging and to 1 V during charging. All full cells with NMC811 as the cathode were cycled with a voltage window of 3–4.2 V, except during extraction cycles. In Gr||NMC811 type cells, three activation cycles were cycled at 0.1C and followed by a CC charge-discharge protocol at 0.5C. Anode-free NMC811-type cells were fabricated with 50 μL of LPF electrolyte, and two activation cycles at 0.1C were included in the initial stage. The CCCV protocol was employed for anode-free cells to extract more Li during charging, and it was composed of 0.2C charge—4.2 V hold to 0.05C–0.3C discharge steps. All electrochemical experiments were conducted at room temperature.

RESOURCE AVAILABILITY

Lead contact

Requests for further information and resources should be directed to, and will be fulfilled by, the lead contact, Yi Cui (yicui@stanford.edu).

Materials availability

This study did not generate any new, unique reagents.

Data and code availability

- Data reported in this paper will be shared by the lead contact upon request.
- This paper does not report original code.

ACKNOWLEDGMENTS

We acknowledge the support of the Assistant Secretary for Energy Efficiency and Renewable Energy, Office of Vehicle Technologies, of the U.S. Department of Energy (DOE) under the Battery Materials Research Program and the Battery500 Consortium program. J.H.L. acknowledges the support from Kwanjeong Education Foundation for the Overseas Graduate Scholarship. Computational work was performed on the Sherlock cluster at Stanford University and on resources of the National Energy Research Scientific Computing Center, supported by the U.S. DOE, Office of Science, under contract no. DE-AC02-05CH11231. We appreciate valuable feedback from Stacey F. Bent and Zhenan Bao on the manuscript. We thank Angela Cai for technical assistance with XPS during the revision of this manuscript.

AUTHOR CONTRIBUTIONS

J.H.L. and Y.C. conceived the idea of the project. J.H.L. conducted synthesis and electrochemical experiments with help from Y.Y. J.H.L. performed SEM experiments. W.Z. conducted *operando* OM and TEM characterizations. S.E.H. helped with XRD characterizations and refinements. S.B.S. conducted XPS experiments. E.G.L. and M.K. conducted DFT simulations. J.L. and D.L. helped process experimental data. I.R.C. helped with the preparation of electrolytes. H.A. helped with the fabrication of freestanding graphite electrodes. Y.Y., S.C.K., M.S.K., J.L., P.S., and S.T.O. helped with data analysis. J.H.L. and Y.C. wrote the manuscript. Y.C. and T.P.D. supervised the project. All authors contributed to the discussion of the paper.

DECLARATION OF INTERESTS

The authors declare no competing interests.

SUPPLEMENTAL INFORMATION

Supplemental information can be found online at https://doi.org/10.1016/j.joule.2026.102632.

Received: March 25, 2026
Revised: June 25, 2026
Accepted: July 23, 2026

REFERENCES

1. Turnbull, D. (1981). Metastable Structures in Metallurgy. Metall. Trans. B *12*, 217–230. https://doi.org/10.1007/BF02654454.

2. McLeod, A.S., Zhang, J., Gu, M.Q., Jin, F., Zhang, G., Post, K.W., Zhao, X.G., Millis, A.J., Wu, W.B., Rondinelli, J.M., et al. (2020). Multi-messenger nanoprobes of hidden magnetism in a strained manganite. Nat. Mater. *19*, 397–404. https://doi.org/10.1038/s41563-019-0533-y.

3. Nova, T.F., Disa, A.S., Fechner, M., and Cavalleri, A. (2019). Metastable ferroelectricity in optically strained $SrTiO_3$. Science *364*, 1075–1079. https://doi.org/10.1126/science.aaw4911.

4. Spencer, M.S. (1986). Stable and metastable metal surfaces in heterogeneous catalysis. Nature *323*, 685–687. https://doi.org/10.1038/323685a0.

5. Tarascon, J.M., and Armand, M. (2001). Issues and challenges facing rechargeable lithium batteries. Nature *414*, 359–367. https://doi.org/10.1038/35104644.

6. Fang, C., Li, J., Zhang, M., Zhang, Y., Yang, F., Lee, J.Z., Lee, M.H., Alvarado, J., Schroeder, M.A., Yang, Y., et al. (2019). Quantifying inactive lithium in lithium metal batteries. Nature *572*, 511–515. https://doi.org/10.1038/s41586-019-1481-z.

7. Moretti, A., Sharova, V., Carvalho, D.V., Boulineau, A., Porcher, W., de Meatza, I., and Passerini, S. (2019). A Comparison of Formation Methods for Graphite//LiFePO4 Cells. Batter, Supercaps *2*, 240–247. https://doi.org/10.1002/batt.201800109.

8. Aurbach, D., Ein-Eli, Y., Markovsky, B., Zaban, A., Luski, S., Carmeli, Y., and Yamin, H. (1995). The Study of Electrolyte Solutions Based on Ethylene and Diethyl Carbonates for Rechargeable Li Batteries: II. Graphite Electrodes. J. Electrochem. Soc. *142*, 2882–2890. https://doi.org/10.1149/1.2048659.

9. Wang, D.Y., Sinha, N.N., Petibon, R., Burns, J.C., and Dahn, J.R. (2014). A systematic study of well-known electrolyte additives in $LiCoO_2$/graphite pouch cells. J. Power Sources *251*, 311–318. https://doi.org/10.1016/j.jpowsour.2013.11.064.

10. Ren, X., Zou, L., Cao, X., Engelhard, M.H., Liu, W., Burton, S.D., Lee, H., Niu, C., Matthews, B.E., Zhu, Z., et al. (2019). Enabling High-Voltage Lithium-Metal Batteries under Practical Conditions. Joule *3*, 1662–1676. https://doi.org/10.1016/j.joule.2019.05.006.

11. Yu, Z., Wang, H., Kong, X., Huang, W., Tsao, Y., Mackanic, D.G., Wang, K., Wang, X., Huang, W., Choudhury, S., et al. (2020). Molecular design for electrolyte solvents enabling energy-dense and long-cycling lithium metal batteries. Nat. Energy *5*, 526–533. https://doi.org/10.1038/s41560-020-0634-5.

12. Kim, M.S., Zhang, Z., Rudnicki, P.E., Yu, Z., Wang, J., Wang, H., Oyakhire, S.T., Chen, Y., Kim, S.C., Zhang, W., et al. (2022). Suspension electrolyte with modified Li+ solvation environment for lithium metal batteries. Nat. Mater. *21*, 445–454. https://doi.org/10.1038/s41563-021-01172-3.

13. Kim, S.C., Wang, J., Xu, R., Zhang, P., Chen, Y., Huang, Z., Yang, Y., Yu, Z., Oyakhire, S.T., Zhang, W., et al. (2023). High-entropy electrolytes for practical lithium metal batteries. Nat. Energy *8*, 814–826. https://doi.org/10.1038/s41560-023-01280-1.

14. Cheng, X.-B., Zhang, R., Zhao, C.-Z., and Zhang, Q. (2017). Toward Safe Lithium Metal Anode in Rechargeable Batteries: A Review. Chem. Rev. *117*, 10403–10473. https://doi.org/10.1021/acs.chemrev.7b00115.

15. Tikekar, M.D., Choudhury, S., Tu, Z., and Archer, L.A. (2016). Design principles for electrolytes and interfaces for stable lithium-metal batteries. Nat. Energy *1*, 16114. https://doi.org/10.1038/nenergy.2016.114.

16. Yu, Z., Cui, Y., and Bao, Z. (2020). Design Principles of Artificial Solid Electrolyte Interphases for Lithium-Metal Anodes. Cell Rep. Phys. Sci. *1*, 100119. https://doi.org/10.1016/j.xcrp.2020.100119.

17. Lin, D., Liu, Y., Liang, Z., Lee, H.W., Sun, J., Wang, H., Yan, K., Xie, J., and Cui, Y. (2016). Layered reduced graphene oxide with nanoscale interlayer gaps as a stable host for lithium metal anodes. Nat. Nanotechnol. *11*, 626–632. https://doi.org/10.1038/nnano.2016.32.

18. Chen, H., Yang, Y., Boyle, D.T., Jeong, Y.K., Xu, R., de Vasconcelos, L.S., Huang, Z., Wang, H., Wang, H., Huang, W., et al. (2021). Free-standing ultrathin lithium metal–graphene oxide host foils with controllable thickness for lithium batteries. Nat. Energy *6*, 790–798. https://doi.org/10.1038/s41560-021-00833-6.

19. Wang, F., Wang, B., Li, J., Wang, B., Zhou, Y., Wang, D., Liu, H., and Dou, S. (2021). Prelithiation: A Crucial Strategy for Boosting the Practical Application of Next-Generation Lithium Ion Battery. ACS Nano *15*, 2197–2218. https://doi.org/10.1021/acsnano.0c10664.

20. Sun, Y., Lee, H.W., Seh, Z.W., Liu, N., Sun, J., Li, Y., and Cui, Y. (2016). High-capacity battery cathode prelithiation to offset initial lithium loss. Nat. Energy *1*, 15008. https://doi.org/10.1038/nenergy.2015.8.

21. Shanmukaraj, D., Grugeon, S., Laruelle, S., Douglade, G., Tarascon, J.M., and Armand, M. (2010). Sacrificial salts: Compensating the initial charge irreversibility in lithium batteries. Electrochem. Commun. *12*, 1344–1347. https://doi.org/10.1016/j.elecom.2010.07.016.

22. Zhao, J., Lu, Z., Liu, N., Lee, H.W., McDowell, M.T., and Cui, Y. (2014). Dry-air-stable lithium silicide-lithium oxide core-shell nanoparticles as high-capacity prelithiation reagents. Nat. Commun. *5*, 5088. https://doi.org/10.1038/ncomms6088.

23. Wu, Z., Ji, S., Zheng, J., Hu, Z., Xiao, S., Wei, Y., Zhuo, Z., Lin, Y., Yang, W., Xu, K., et al. (2015). Prelithiation Activates Li(Ni0.5Mn0.3Co0.2)O2 for High Capacity and Excellent Cycling Stability. Nano Lett. *15*, 5590–5596. https://doi.org/10.1021/acs.nanolett.5b02246.

24. Yang, C., Ma, H., Yuan, R., Wang, K., Liu, K., Long, Y., Xu, F., Li, L., Zhang, H., Zhang, Y., et al. (2023). Roll-to-roll prelithiation of lithium-ion battery anodes by transfer printing. Nat. Energy *8*, 703–713. https://doi.org/10.1038/s41560-023-01272-1.

25. Yang, Y., Wang, J., Kim, S.C., Zhang, W., Peng, Y., Zhang, P., Vilá, R.A., Ma, Y., Jeong, Y.K., and Cui, Y. (2023). In Situ Prelithiation by Direct Integration of Lithium Mesh into Battery Cells. Nano Lett. *23*, 5042–5047. https://doi.org/10.1021/acs.nanolett.3c00859.

26. Lin, L., Qin, K., Zhang, Q., Gu, L., Suo, L., Hu, Y.S., Li, H., Huang, X., and Chen, L. (2021). Li-Rich Li2 [Ni0.8 Co0.1 Mn0.1]O2 for Anode-Free Lithium Metal Batteries. Angew. Chem. Int. Ed. *60*, 8289–8296. https://doi.org/10.1002/anie.202017063.

27. Okamoto, H. (2011). Cu-Li (Copper-Lithium). J. Phase Equilib. Diffus. *32*, 172. https://doi.org/10.1007/s11669-010-9840-3.

28. Gu, X., Dong, J., and Lai, C. (2021). Li-containing alloys beneficial for stabilizing lithium anode: A review. Eng. Rep. *3*, e12339. https://doi.org/10.1002/eng2.12339.

29. Jia, W., Liu, Y., Wang, Z., Qing, F., Li, J., Wang, Y., Xiao, R., Zhou, A., Li, G., Yu, X., et al. (2020). Low-temperature fusion fabrication of Li-Cu alloy anode with in situ formed 3D framework of inert $LiCu_x$ nanowires for excellent Li storage performance. Sci. Bull. *65*, 1907–1915. https://doi.org/10.1016/j.scib.2020.07.012.

30. Lu, Z., Tai, Z., Yu, Z., LaGrow, A.P., Bondarchuk, O., Sousa, J.P.S., Meng, L., Peng, Z., and Liu, L. (2021). Lithium–copper alloy embedded in 3D porous copper foam with enhanced electrochemical performance toward lithium metal batteries. Mater. Today Energy *22*, 100871. https://doi.org/10.1016/j.mtener.2021.100871.

31. Rupp, R., Caerts, B., Vantomme, A., Fransaer, J., and Vlad, A. (2019). Lithium Diffusion in Copper. J. Phys. Chem. Lett. *10*, 5206–5210. https://doi.org/10.1021/acs.jpclett.9b02014.

32. Rehnlund, D., Lindgren, F., Böhme, S., Nordh, T., Zou, Y., Pettersson, J., Bexell, U., Boman, M., Edström, K., and Nyholm, L. (2017). Lithium trapping in alloy forming electrodes and current collectors for lithium based batteries. Energy Environ. Sci. *10*, 1350–1357. https://doi.org/10.1039/c7ee00244k.

33. Gąsior, W., Onderka, B., Moser, Z., Dębski, A., and Gancarz, T. (2009). Thermodynamic evaluation of Cu-Li phase diagram from EMF measurements and DTA study. Calphad *33*, 215–220. https://doi.org/10.1016/j.calphad.2008.10.006.

34. Adair, K.R., Iqbal, M., Wang, C., Zhao, Y., Banis, M.N., Li, R., Zhang, L., Yang, R., Lu, S., and Sun, X. (2018). Towards high performance Li metal batteries: Nanoscale surface modification of 3D metal hosts for pre-stored

Li metal anodes. Nano Energy *54*, 375–382. https://doi.org/10.1016/j.nanoen.2018.10.002.

35. Suryanarayana, C., and Norton, M.G. (1998). X-Ray Diffraction (Springer). https://doi.org/10.1007/978-1-4899-0148-4.
36. Kartamyshev, A.I., Poletaev, D.O., Boev, A.O., and Aksyonov, D.A. (2023). Weak segregation and accelerated diffusion of Li at twin boundaries in Cu from DFT: Implications for current collectors in Li-ion batteries. Comput. Mater. Sci. *230*, 112517. https://doi.org/10.1016/j.commatsci.2023.112517.
37. Zhang, W., Sayavong, P., Xiao, X., Oyakhire, S.T., Shuchi, S.B., Vilá, R.A., Boyle, D.T., Kim, S.C., Kim, M.S., Holmes, S.E., et al. (2024). Recovery of isolated lithium through discharged state calendar ageing. Nature *626*, 306–312. https://doi.org/10.1038/s41586-023-06992-8.
38. Hou, T., Yang, G., Rajput, N.N., Self, J., Park, S.W., Nanda, J., and Persson, K.A. (2019). The influence of FEC on the solvation structure and reduction reaction of LiPF6/EC electrolytes and its implication for solid electrolyte interphase formation. Nano Energy *64*, 103881. https://doi.org/10.1016/j.nanoen.2019.103881.
39. Ai, H., Cai, A., Holoubek, J., Zhang, W., Greenburg, L.C., Lee, J., Holmes, S., Suzuki, Y., Kuwajima, H., Matsumoto, R., et al. (2025). Homogeneous 3D Porous Conductive Electrodes for High-Energy Battery Fast Charging. ACS Energy Lett. *10*, 4203–4211. https://doi.org/10.1021/acsenergylett.5c01406.
40. Kresse, G., and Furthmü, J. (1996). Efficient iterative schemes for ab initio total-energy calculations using a plane-wave basis set. Phys. Rev. B Condens. Matter *54*, 11169–11186.
41. Blochl, P.E. (1996). Projector augmented-+rave method. Phys. Rev. B *50*, 16533–16539.
42. Perdew, J.P., Burke, K., and Wang, Y. (1996). Generalized gradient approximation for the exchange-correlation hole of a many-electron system. Phys. Rev. B Condens. Matter *54*, 16533–16539. https://doi.org/10.1103/PhysRevB.54.16533.